European Journal of Nuclear Medicine and Molecular Imaging (2025) 52:1631–1641
https://doi.org/10.1007/s00259-024-07044-7

ORIGINAL ARTICLE

JHU-2545 preferentially shields salivary glands and kidneys during PSMA-targeted imaging

Michael T. Nedelcovych[1,2,13] · Ranjeet P. Dash[1,2] · Ying Wu[1] · Eun Yong Choi[3] · Rena S. Lapidus[3] · Pavel Majer[4] · Andrej Jančařík[4] · Diane Abou[5] · Marie-France Penet[6,7] · Anastasia Nikolopoulou[8] · Alex Amor-Coarasa[8] · John Babich[8] · Daniel L. Thorek[5] · Rana Rais[1,2] · Clemens Kratochwil[9] · Barbara S. Slusher[1,2,6,10,11,11,12,13]

Received: 11 June 2024 / Accepted: 16 December 2024 / Published online: 2 January 2025

Abstract

Purpose Prostate-specific membrane antigen (PSMA) radioligand therapy is a promising treatment for metastatic castration-resistant prostate cancer (mCRPC). Several beta or alpha particle-emitting radionuclide-conjugated small molecules have shown efficacy in late-stage mCRPC and one, [[177Lu]Lu]Lu-PSMA-617, is FDA approved. In addition to tumor upregulation, PSMA is also expressed in kidneys and salivary glands where specific uptake can cause dose-limiting xerostomia and potential for nephrotoxicity. The PSMA inhibitor 2-(phosphonomethyl)pentanedioic acid (2-PMPA) can prevent kidney uptake in mice, but also blocks tumor uptake, precluding its clinical utility. Preferential delivery of 2-PMPA to non-malignant tissues could improve the therapeutic window of PSMA radioligand therapy.

Methods A tris(isopropoxycarbonyloxymethyl) (TrisPOC) prodrug of 2-PMPA, JHU-2545, was synthesized to enhance 2-PMPA delivery to non-malignant tissues. Mouse pharmacokinetic experiments were conducted to compare JHU-2545-mediated delivery of 2-PMPA to plasma, kidney, salivary glands, and C4-2 prostate tumor xenograft. Imaging studies were conducted in rats and mice to measure uptake of PSMA PET tracers in kidney, salivary glands, and prostate tumor xenografts with and without JHU-2545 pre-treatment.

Results JHU-2545 resulted in approximately 3- and 53-fold greater exposure of 2-PMPA in rodent salivary glands (18.0 ± 0.97 h*nmol/g) and kidneys (359 ± 4.16 h*nmol/g) versus prostate tumor xenograft (6.79 ± 0.19 h*nmol/g). JHU-2545 also blocked rodent kidneys and salivary glands uptake of the PSMA PET tracers [68Ga]Ga-PSMA-11 and [18 F] F-DCFPyL by up to 85% with little effect on tumor.

Conclusions JHU-2545 pre-treatment may enable greater cumulative administered doses of PSMA radioligand therapy, possibly improving safety and efficacy.

Key points

Question: Is there a method of limiting PSMA radioligand uptake into salivary glands and kidneys to potentially mitigate associated toxicity without hindering tumor uptake/efficacy?

Pertinent findings: JHU-2545, a prodrug of the PSMA inhibitor 2-PMPA, was found to preferentially deliver 2-PMPA to salivary glands and kidneys relative to tumor xenografts in rodent models, leading to blunted uptake of PSMA radioligands in non-tumor tissues.

Implications for patient care: If replicated in clinical studies, JHU-2545 could reduce radiation doses to salivary glands and kidneys and possibly mitigate associated toxicities in prostate cancer patients receiving PSMA radioligand therapy.

Keywords PSMA · Radioligand therapy · Prostate cancer · Kidneys · Salivary glands

Extended author information available on the last page of the article

Introduction

PSMA radioligand therapy has emerged as a promising treatment for mCRPC [1–3] with one agent, lutetium Lu 177 vipivotide tetraxetan ([177Lu]Lu-PSMA-617), approved for use in late-stage patients after demonstrating survival benefit in a Phase 3 trial [4, 5]. This approach is based on the observation that PSMA is highly upregulated (10–100 fold) in the majority of prostate cancer lesions [6, 7], and though its functional role in malignancy is unclear, the degree to which PSMA surface expression is increased correlates with disease progression, androgen independence, and metastasis [6, 7]. Ligand binding to PSMA induces rapid internalization, enriching the agent inside the cell and promoting accumulation within PSMA-expressing tissues [6, 7].

In addition to PSMA-617, multiple small molecule PSMA ligands are in clinical development for prostate cancer imaging and radioligand therapy. These molecules are conjugated to diagnostic or therapeutic particle-emitting radionuclides suitable for PET imaging (e.g. piflufolastat F18/[18 F]F-DCFPyL, gallium Ga 68 gozetotide/[68Ga]Ga-PSMA-11, [68Ga]Ga-PSMA-617), beta therapy (e.g. [177Lu]Lu-PSMA-617, [177Lu]Lu-PSMA-I&T, ^{131}I-MIP-1095, [177Lu]Lu-rhPSMA), or alpha therapy (e.g. [225Ac]Ac-PSMA-617, [225Ac]Ac-PNT2002) [8–11]. The theranostic paradigm of PSMA radioligand therapy benefits from the capability to confirm and quantitate PSMA expression in malignant tissues by PET. Indeed, [177Lu]Lu-PSMA-617 is approved for use in the U.S. only in patients with PSMA-positive mCRPC based on PET imaging with [68Ga]Ga-PSMA-11 or another approved PSMA-11 imaging agent [5].

Despite significant progress, clinical development of PSMA-targeted agents is complicated by the physiologic expression of PSMA in normal tissues including salivary glands and kidneys [12–16] which exhibit avid uptake of PSMA radiopharmaceuticals during imaging and radioligand therapy [7, 10]. Salivary gland uptake of PSMA radioligands can result in transient or permanent xerostomia, an adverse effect particularly problematic for alpha radionuclides [2, 17]. For example, [225Ac]Ac-PSMA-617 showed efficacy in heavily pre-treated mCRPC patients (5/40 complete tumor control > 2 years), but this response was nearly matched by treatment discontinuation due to debilitating xerostomia (4/40) [2]. Clinical studies of PSMA radioligands labeled with Actinium-225 have found meaningful clinical activity even in patients previously treated with a Lutetium-177 agent. Xerostomia, however, is typically more frequent and more severe [18, 19]. Experience with [177Lu]Lu-PSMA-617 reveals high rates of xerostomia that is generally low-grade.

Cumulative kidney absorbed dose brings the potential risk of nephrotoxicity that could restrict the number of allowable cycles [6, 7, 13, 20–26]. Repeated cycles have been associated with improved efficacy and response rate, suggesting that this limitation could result in sub-optimal outcomes [13, 27–31]. Significant deleterious effects on kidney function have not yet been closely associated with beta emitting PSMA radioligands [26, 30], but this consideration may become more relevant as attempts are made to move these agents earlier in the prostate cancer treatment paradigm. Potential combination or sequencing of beta and alpha emitters may also heighten concern around nephrotoxicity [18, 31].

In an attempt to mitigate healthy tissue exposure during PSMA radioligand therapy, the highly selective PSMA inhibitor 2-PMPA ($IC_{50} = 0.3$nM) has been evaluated for its ability to block radioligand uptake in the salivary glands and kidneys through direct competitive displacement at a shared PSMA binding site [21, 24]. In one study, 2-PMPA (0.01 mg) co-injection with [177Lu]Lu-PSMA I&T (100 MBq) reduced the absorbed dose to the kidneys by 83% and attenuated nephrotoxicity at 3 months post-treatment in mice bearing PSMA-expressing xenografts [24]. Although encouraging, these results did not prompt clinical testing because 2-PMPA also inhibited tumor uptake of the radioligand > 50%, resulting in accelerated tumor growth and significantly reduced overall survival relative to mice that received the radioligand alone [24]. Similar results were obtained when 2-PMPA was paired with ^{125}I-MIP-1095 [21]. Thus, although 2-PMPA provided an important proof-of-concept for the shielding approach, co-treatment with this molecule could not strike a balance between salivary gland/kidney displacement versus tumor uptake that could improve the therapeutic index of PSMA radioligand therapy.

Herein we describe the use of a tris(isopropoxycarbonyl oxymethyl) (TrisPOC) 2-PMPA prodrug termed JHU-2545, which preferentially delivers 2-PMPA to non-malignant tissues such as salivary glands and kidneys. In rodent pharmacokinetic studies, JHU-2545 exhibited 2.65- and 52.9-fold enhanced delivery of 2-PMPA to salivary glands and kidneys, respectively, versus prostate cancer xenografts. In further support of this finding, pre-treatment with JHU-2545 was shown to block [68Ga]Ga-PSMA-11 uptake in rat kidneys and [18 F]F-DCFPyL uptake in mouse salivary glands and kidneys by up to 85% without substantial effect on prostate cancer xenograft uptake. JHU-2545 pre-treatment may thus raise the cumulative dose limit and improve the safety and efficacy of PSMA radioligand therapy.

Materials and methods

Cell culture

22RV1 cells were verified by short tandem repeat profiling (American Type Culture Collection), grown in RPMI-1640 (Thermo Fisher Scientific), and passaged in 0.25% Trypsin prior to sterile collection for animal studies.

Animals

All animal experiments were conducted in compliance with National Institutes of Health (NIH) guidelines and with the approval of the Institutional Animal Care and Use Committees at Johns Hopkins University, the University of Maryland, and Weill Cornell Medicine and were undertaken in accordance with the guidelines set forth by the United States Public Health Service Policy on Humane Care and Use of Laboratory Animals. All rodents were maintained on a 12 h light-dark cycle with unrestricted access to food and water. Adult male Sprague-Dawley rats (500–550 g) were obtained from Taconic and used for [68Ga]Ga-PSMA-11 PET imaging studies. Adult male 8 wk FVB and Nu/Nu mice were used for [18 F]F-DCFPyL PET studies. Nu/Nu mice were implanted with 5×10^6 22RV1 cells in a 1:1 PBS: matrigel mixture and allowed to grow to approximately 250 mm^3 (3 weeks). Adult male Non-obese diabetic scid gamma (NSG) mice (UMB Vet Resources) were used for pharmacokinetic experiments. To generate a C4-2 in vivo model, 3×10^6 LNCaP-C4-2 cells (kind gift of Miriam Smith PhD, University of Maryland School of Medicine) were subcutaneously injected into the flanks of male NSG mice. When tumors grew to approximately 600–800 mm^3, tumors were excised, aseptically cut into 2 mm x 2 mm pieces and frozen back viably (5% DMS0/95% FBS). Tumors were not passaged from mouse to mouse more than 4 times. For the current experiment, two vials of viably frozen explants were thawed at 37 °C. Tumor explants were washed in RPMI without FCS and then surgically implanted in a subcutaneous pocket in male NSG mice. When tumors reached 600–800 mm^3, mice were euthanized, tumors excised aseptically, and cut into 2 mm x 2 mm pieces prior to re-implantation into 40 mice. When tumors reached 500–700 mm^3, the pharmacokinetic experiment was performed.

Compounds

2-PMPA was obtained from Sigma Aldrich (St. Louis, MO). JHU-2545 was synthesized and characterized as previously described by our group (Compound 21b) [32]. Clinical-grade [18 F]F-DCFPyL was formulated under good manufacturing practices as previously described [33, 34] at the Johns Hopkins University School of Medicine PET Center (at specific activities of approximately 111 GBq/μmol). Gallium-68-labeled tracers were all prepared at the Citigroup Biomedical Imaging Center (CBIC) radiochemistry facility at Cornell according to the methods described in [35].

Mouse pharmacokinetics

2-PMPA (3 mg/kg, i.v.) or a molar equivalent of JHU-2545 (7.62 mg/kg, i.v.) were injected via tail vein after dissolution in vehicle (5% EtOH/10% Tween 80/ 85% 50mM HEPES). Mice were then euthanized under isoflurane anesthesia 0.25, 0.5, 1, 3, or 6 h post-dose ($n=3$/group). Blood was collected by cardiac puncture into EDTA-lined tubes and stored on ice until plasma was isolated by centrifugation. Salivary glands, kidneys, and tumor were harvested and flash frozen on dry ice. All tissues were stored at -80 °C prior to bioanalysis.

Rodent PET imaging

PET acquisitions for rat [68Ga]Ga-PSMA-11 were performed with a Biograph mCT scanner (Siemens Healthcare, Malvern, PA, USA) in groups of 4 animals. Rats were anesthetized with isoflurane (Henry Schein Animal Health, Melville, NY) at 2-2.5% in oxygen for induction, and 1.5-2% in oxygen for maintenance. After induction of anesthesia, an i.v. catheter was inserted into the tail vein of each rat. The animals were then positioned in the camera in transaxial position with its body in the center of the field of view. Thirty minutes before radiotracer administration, rats were treated with either vehicle or JHU-2545 at 1 or 10 mg/kg of body weight via the i.v. catheter (0.5 mL/rat, $n=2$/group). JHU-2545 stock solution was prepared in 10% EtOH in PBS. [68Ga]Ga-PSMA-11 (42 ± 5 MBq/rat) was injected as a bolus (~0.5 mL) and a 60-min dynamic scan started with 12×5 min time frames. For all the acquisitions, a CT scan of 8.9 s was performed before PET, for attenuation correction. The list-mode data were iteratively reconstructed with TrueX + TOF (UltraHD PET) (2 iterations, 21 subsets) after being normalized and corrected for attenuation, scatter and decay with final images having a voxel size of 2.06 mm ($2.0\times1.02\times1.02$). Volumes of Interest (VOIs) were manually drawn onto the dynamic PET images to extract time-activity curves and %ID/g values. All image analyses were performed using the AMIDE software. Mice undergoing [18 F]F-DCFPyL PET imaging were administered radiotracer (7.4-9 MBq) either anesthetized (isoflurane) on camera with a tail vein catheter for kinetic studies, or via the retroorbital sinus for static images. A dedicated high resolution small animal PET scanner (R4, Concorde Microsystems; 7.8 cm axial by 10 cm transaxial field of view) was used to acquire whole body scans (in the prone

position) in list-mode configuration with a 350–700 keV energy range and a coincidence-timing window of 6 nsec for a minimum of 20×10^6 coincident events as previously described [36]. PET image data were corrected for detector non-uniformity, dead time, random coincidences and physical decay and normalized to injected activity (determined by Capintec CR15 dose calibrator with setting #457). All images were reconstructed using the 3D maximum a posteriori (3D-MAP) algorithm. ASIPro software (Siemens) was used to place three-dimensional regions of interest volumes of interest at the regions of the tumors, salivary glands, heart and kidneys for analysis. Time-activity curves were generated after administration of vehicle or JHU-2545 (5 mg/kg, i.v.) 5–60 min prior to [18 F]F-DCFPyL bolus dosing ($n = 2$–3/group). JHU-2545 dose effects were assessed by administration of vehicle or JHU-2545 (0.05-5 mg/kg, i.v.) 15 min prior to [18 F]F-DCFPyL bolus dosing ($n = 2$–3/group).

Bioanalysis

Bioanalysis to determine 2-PMPA concentrations after protein precipitation was conducted by LC–MS/MS as previously described [32, 37]. 2-PMPA standard curves (10–50,000 nM) were prepared in the appropriate matrix tissue. For plasma, protein extraction was performed by addition of 50 uL of calibration standard or sample into silanized vials prior to mixing with 300 uL of methanol with internal standard and centrifugation at 12,000 g for 10 min. Supernatant was then transferred to a new tube and evaporated to dryness at 40 °C under a gentle stream of nitrogen. For solid tissues, samples were incubated 1:5 w/v with methanol, stored at − 20 °C for 1 h, and then homogenized. Homogenized samples were centrifuged at 12,000 g for 10 min; 100 µL of the supernatant was then mixed with 100 µL of internal standard in methanol, and then evaporated to dryness as above. 2-PMPA samples and standards were derivatized using N-tert-butyldimethylsilyl-N-methyltrifluoroacetamide with 1% tert-butyldimethylchlorosilane (MTBSTFA + 1% TBDMSCl), to enable reverse phase chromatography, as previously described [32, 37]. Briefly, samples and standards were reconstituted in 100 µL acetonitrile to which 50 µL of MTBSTFA was added and set to react at 60 °C in a water bath for 30 min. Upon completion of the reaction, the samples were then centrifuged again at 10,000 rpm at 5 °C for 2 min. 100 µL of supernatant was transferred to 250 µL of polypropylene autosampler vials sealed with Teflon caps and analyzed via LC–MS/MS. Separation of the analyte was achieved using a Waters X-terra, RP18, 3.5 µm, and 2.1×50 mm. The mobile phase was composed of 0.1% formic acid in acetonitrile and 0.1% formic acid in H_2O with gradient elution. Chromatographic analysis was performed on an Accela UPLC and a TSQ vantage mass spectrometer. The $[M+H]^+$ ion transitions of derivatized 2-PMPA at m/z 683.0 → 551.4 and that of the internal standard at m/z 669.0 → 537.2 were monitored.

Pharmacokinetic and statistical analysis

Non-compartmental-analysis module in Phoenix WinNonlin version 7.0 (Certara USA, Inc., Princeton, NJ) was used to assess pharmacokinetic parameters. Peak plasma concentrations (C_{max}) were the observed values. Area under the curve (AUC) was calculated by log–linear trapezoidal rule to the end of sample collection (AUC_{last}). Comparisons between rat kidney uptake of [68Ga]Ga-PSMA-11 were conducted by one-way ANOVA with Dunnett's post hoc test. Comparisons between mouse kidney, salivary gland, and tumor uptake of [18 F]F-DCFPyL were conducted by two-tailed *t*-test. Significance was defined as $P < 0.05$.

Results

JHU-2545 preferentially delivered 2-PMPA to mouse salivary glands and kidneys versus prostate cancer xenograft

Concentrations of 2-PMPA in plasma, tumor, salivary glands, and kidneys were measured at multiple time points after tail vein administration of either 2-PMPA or JHU-2545 (3 mg/kg or molar equivalent, i.v.) to NSG mice harboring subcutaneous xenografts of human C4-2 prostate cancer cells. JHU-2545 administration resulted in 2-PMPA plasma, kidney, and salivary gland exposures of 17.8 ± 1.02 h*nmol/mL, 359 ± 4.16 h*nmol/g, and 18.0 ± 0.97 h*nmol/g, respectively (Fig. 1). Kidney and salivary gland exposures were 52.9- and 2.65-fold greater than those observed in the tumor (6.79 ± 0.19 h*nmol/g) (Fig. 1). When compared to direct 2-PMPA administration, kidney: tumor and salivary: tumor 2-PMPA concentration ratios over time were increased several fold by JHU-2545 with no significant effect on the plasma: tumor ratio (Fig. 2). Administration of 2-PMPA (3 mg/kg, i.v.) resulted in mean 2-PMPA exposures in the tumor, plasma, kidney, and salivary gland of 7.2 ± 1.2 h*nmol/g, 33.5 ± 6.1 h*nmol/mL, 137.5 ± 39.7 h*nmol/g, and 2.7 ± 0.4 h*nmol/g, respectively, yielding plasma: tumor, kidney: tumor, and salivary gland: tumor AUC ratios of 4.7, 19.2, and 0.38.

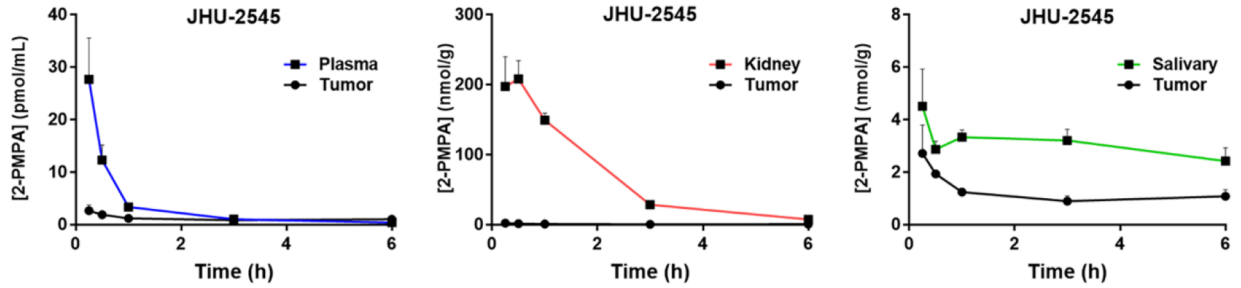

JHU-2545 Pharmacokinetic Parameters

Tissue	C_{max} (nmol/mL or nmol/g)	$AUC_{0\text{-}t}$ (h*nmol/mL or h*nmol/g)	Tissue:Tumor AUC Ratio
Tumor	2.72 ± 0.62	6.79 ± 0.19	1.00
Plasma	27.7 ± 4.55	17.8 ± 1.02	2.62
Salivary	4.63 ± 0.73	18.0 ± 0.97	2.65
Kidney	226 ± 8.26	359 ± 4.16	52.9

Fig. 1 JHU-2545 preferentially delivers 2-PMPA to mouse salivary glands and kidneys versus prostate cancer xenografts. Mice bearing subcutaneous C4-2 prostate cancer xenografts were administered JHU-2545 (3 mg/kg molar equivalent to 2-PMPA, i.v., $n = 3$/group). 2-PMPA concentrations were monitored over time in plasma, kidneys, salivary glands, and tumor xenograft by LC-MS. JHU-2545 administration resulted in substantially higher 2-PMPA exposures in the kidneys and salivary glands compared to tumor. Data represented as mean or mean ± SEM

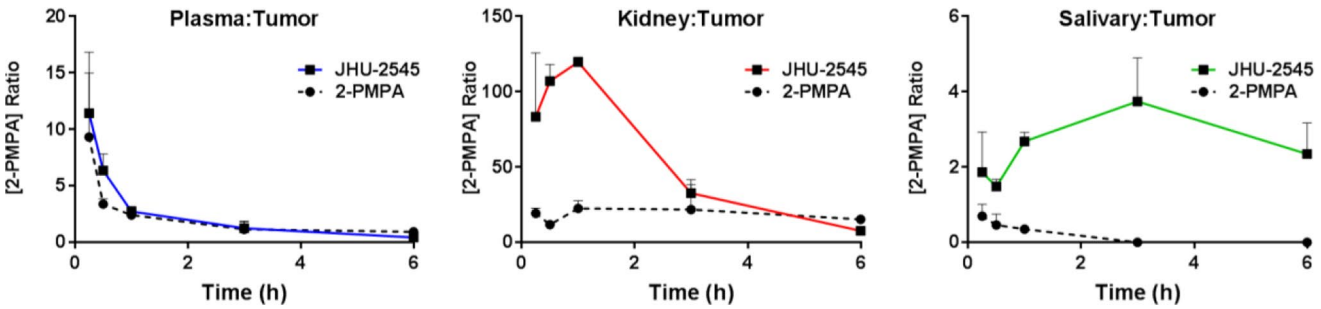

Fig. 2 Mice bearing subcutaneous C4-2 prostate cancer xenografts were administered 2-PMPA (3 mg/kg, i.v.) or equimolar JHU-2545 ($n = 3$/group). 2-PMPA concentrations were monitored over time in plasma, kidneys, salivary glands, and tumor xenograft by LC-MS. Relative to administration of equimolar 2-PMPA, JHU-2545 improved the kidney: tumor and salivary glands: tumor concentration ratios over time without affecting the plasma: tumor ratio. Data represented as mean + SEM

JHU-2545 pre-treatment dose-dependently attenuated uptake of PSMA radioligands in rat kidneys

Kidney shielding was first confirmed by PET imaging after administration of JHU-2545 (1 or 10 mg/kg, i.v.) to rats 30 min prior to [68Ga]Ga-PSMA-11 (42 ± 5 MBq) bolus dosing. PET images clearly showed differences in renal uptake and retention with greater cortical uptake and retention in the saline control animals (Fig. 3A, top) compared with the animals treated with JHU-2545 (Fig. 3A, bottom). In the dynamic PET scans, JHU-2545 treated rats show reduced renal cortical retention of radiotracer compared to controls with rapid flux through the renal pelvis with activity rapidly passing into the bladder. Time activity curves derived from the ROI data (Fig. 3B) show a dose effect with a modest drop in activity at 1 mg/kg JHU-2545 and a more dramatic effect at 10 mg/kg JHU-2545. Using the trapezoid method, area under the curve for each treatment arm was calculated; compared to controls, there was a significant reduction of 20% and 69% in the integrated kidney dose at

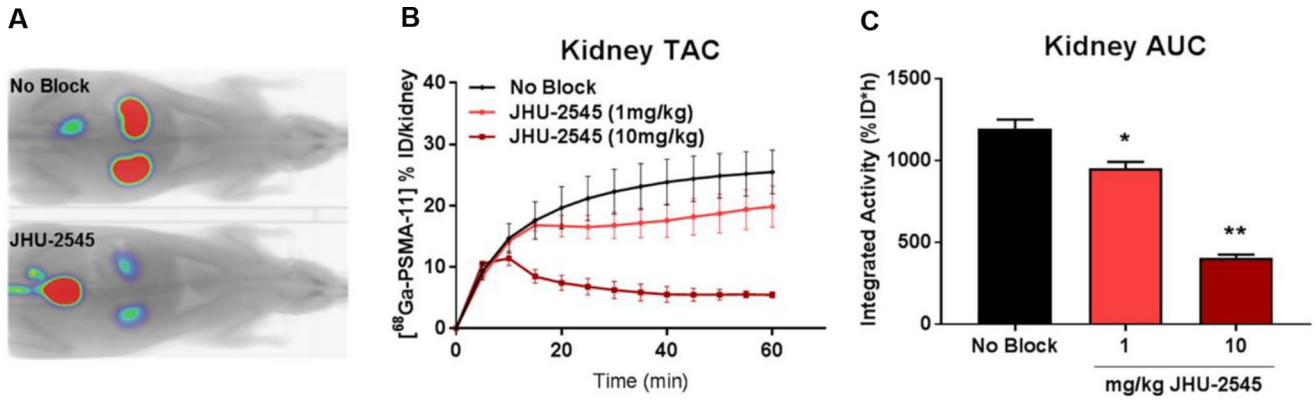

Fig. 3 JHU-2545 pre-treatment dose-dependently attenuated uptake of ^{68}Ga-PSMA-11 in rat kidneys. JHU-2545 (1 or 10 mg/kg, i.v.) or saline was administered to rats 30 min prior to ^{68}Ga-PSMA-11 (42 ± 5 MBq) bolus dosing (n = 2/group). (**A**) PET images showed greater cortical renal uptake in control animals (top) compared to animals treated with JHU-2545 (bottom). JHU-2545 treated rats show rapid renal flux with activity passing into the bladder. (**B**) Time activity curves (TAC) show a dose-dependent effect. (**C**) Quantification using the trapezoid method shows a significant, dose-dependent reduction in ^{68}Ga-PSMA-11 area under the curve (AUC). Data represented as mean ± SEM; *$p < 0.05$, **$p < 0.01$

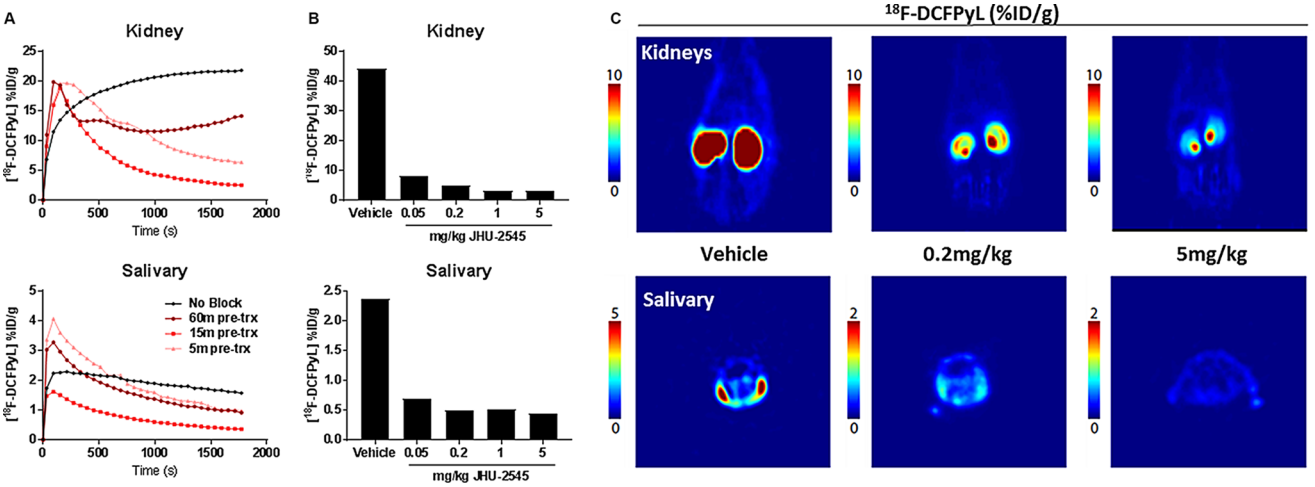

Fig. 4 JHU-2545 pre-treatment attenuated uptake of ^{18}F-DCFPyL in mouse salivary glands and kidneys in dose and time-dependent fashion. (**A**) JHU-2545 (5 mg/kg, i.v.) or vehicle was administered to mice 5, 15, or 60 min prior to ^{18}F-DCFPyL (7.4-9MBq) bolus dosing (n = 2–3/group). Time activity curves showed that 15-minute pre-treatment provides maximal shielding of kidneys and salivary glands. (**B**) JHU-2545 (0.05-5 mg/kg, i.v.) was administered 15 min prior to ^{18}F-DCFPyL bolus dosing (n = 2–3/group). Dose-dependent shielding of kidneys and salivary glands was observed with peak effect between 0.2 and 1 mg/kg. (**C**) Representative PET images of kidneys and salivary glands at the indicated JHU-2545 dose

1 and 10 mg/kg JHU-2545, respectively [F [2, 3] = 95.28; p = 0.0019] (Fig. 3C).

JHU-2545 at a dose of 0.25 mg/kg and a pre-treatment time of 15 min optimally shielded rodent kidneys and salivary glands with no substantial effect on prostate cancer tumor uptake

A dose response (0.05–5 mg/kg, i.v.) and time course (5–60 min pre-treatment) of JHU-2545 was subsequently evaluated for kidney and salivary gland blocking in non-tumor bearing mice assessing uptake of [18 F]F-DCFPyL by PET. Administration of JHU-2545 (5 mg/kg, i.v.) 15 min prior to tracer administration was found to optimally attenuate radioligand uptake in both organs as assessed by time-activity curves (Fig. 4A). With this pre-treatment time, JHU-2545 achieved maximal radioligand shielding in the kidneys and salivary glands between 0.2 and 1 mg/kg (Fig. 4B). Representative PET images at 1 h post-tracer injection exhibit robust, dose-dependent clearance of [18 F]F-DCFPyL from the renal cortex and salivary glands of mice pre-treated with JHU-2545 (Fig. 4C). To ensure minimal interference with tumor uptake, the lowest efficacious dose of JHU-2545 was subsequently used to assess kidney and salivary gland shielding in 22RV1 tumor-bearing mice. When administered 15 min prior to injection of [18 F]

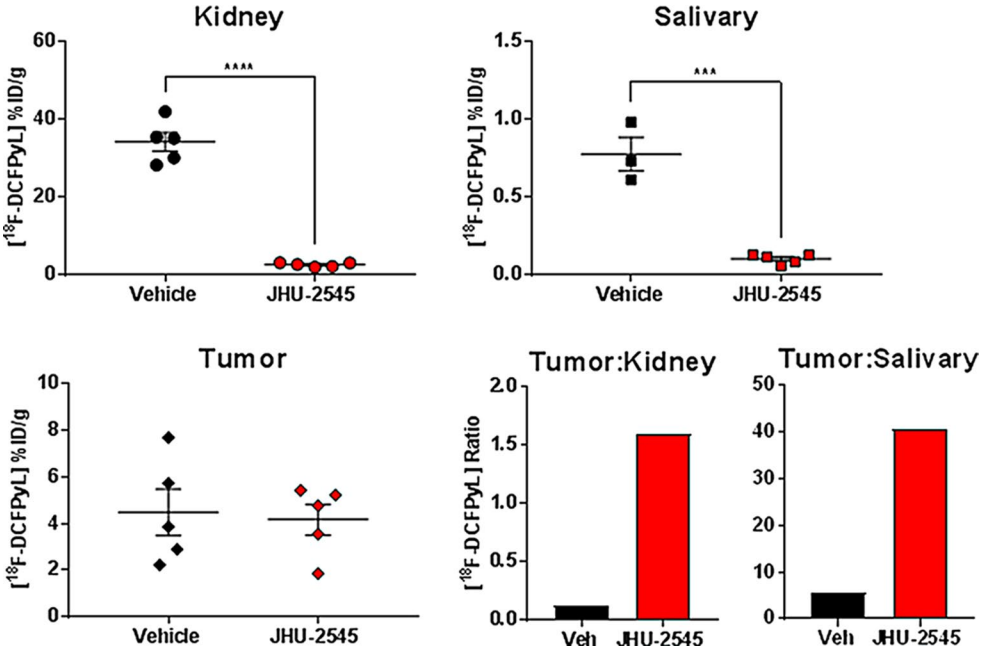

Fig. 5 JHU-2545 pre-treatment attenuated uptake of ^{18}F-DCFPyL in mouse salivary glands and kidneys but not prostate cancer xenografts. JHU-2545 (0.25 mg/kg, i.v.) or vehicle was administered to mice bearing subcutaneous 22RV1 prostate cancer xenografts 15 min prior to ^{18}F-DCFPyL bolus dosing ($n=5$/group). JHU-2545 treatment significantly reduced kidney and salivary gland uptake of ^{18}F-DCFPyL at 1 h post-tracer administration with no effect on tumor xenograft uptake, resulting in increased tumor: kidney and tumor: salivary uptake ratios. Data represented as mean or mean ± SEM; ***$p<0.001$

F-DCFPyL (7.4-9 MBq, i.v.), JHU-2545 (0.25 mg/kg, i.v.) blocked salivary gland and kidney uptake but had no effect on tumor uptake of radioligand at 60 min post-tracer injection relative to mice pre-treated with vehicle (Fig. 5). Vehicle vs. JHU-2545 pre-treatment, respectively, resulted in salivary gland uptake of 0.78 ± 0.19 vs. 0.10 ± 0.03%ID/g [t [6] = 8.27; $p=0.0002$]; kidney uptake of 34.21 ± 5.36 vs. 2.6 ± 0.52%ID/g [t [8] = 13.1; $p<0.0001$]; and tumor uptake of 4.48 ± 2.23 vs. 4.17 ± 1.49%ID/g [t [8] = 0.26; $p=0.7988$] (Fig. 5). JHU-2545 pre-treatment thus afforded 85 and 87% mean reductions in kidney and salivary gland uptake of PSMA radioligand at 60 min, but had no effect on tumor uptake, substantially improving the tumor: kidney and tumor: salivary uptake ratios (Fig. 5). Thus, JHU-2545 at a dose of 0.25 mg/kg and a pre-treatment time of 15 min was found to provide optimal preferential shielding.

Discussion

We have shown that a novel prodrug, JHU-2545, preferentially delivers the PSMA inhibitor 2-PMPA to the salivary glands and kidneys, reducing exposure of these organs to PSMA-inhibitor based radiopharmaceuticals without substantially hindering tumor uptake in some preclinical models. This may be one approach to increasing the therapeutic index of PSMA radioligands [37–43], and potentially enable greater administered activities for larger cumulative absorbed doses to tumor tissues. In contrast to previous studies, which found that direct injection of 2-PMPA shielded prostate cancer as well as normal organs, the approach here appears to preferentially block molecular recognition of PSMA in normal tissues. Furthermore, in the salivary glands, co-treatment with 2-PMPA has previously been found to have no beneficial effect [21], likely owing to poor penetration of this tissue compartment due to the molecule's high polarity [32, 37]. In the current study, relative to direct injection of equimolar 2-PMPA, we show significantly increased 2-PMPA exposure in the salivary glands and kidneys afforded by the prodrug approach with JHU-2545, without meaningfully increasing plasma or tumor exposures.

Other efforts to shift specific uptake of PSMA radiopharmaceuticals to malignant tissues have included structural modification of PSMA-targeting moieties [44–47]. For example, attempts have been made to improve tumor exposure by conjugating PSMA inhibitors to an albumin-binding moiety including PSMA-617 [44, 45], PSMA I&T [47], as well as other urea-based [45] or phosphoramidate-based scaffolds [48]. These analogues exhibited prolonged plasma half-life and delivered larger radiation doses to mCRPC xenografts, but full organ radiation dosimetry in early clinical tests have revealed concurrent increases in kidney and/or salivary gland doses that in some cases translated to even worse tissue: tumor ratios [46, 49, 50].

Wide-ranging but ultimately unsuccessful attempts have also been made to non-specifically mitigate kidney and salivary gland toxicities. These strategies have included co-administration of gelofusine [24] and mannitol [51] to inhibit renal reabsorption, facial application of ice packs to reduce salivary gland blood flow [52], and salivary gland injection of botulinum toxin [53], all of which offered little or no benefit with the exception of botulinum toxin injection. However, this invasive approach has no effect on

kidneys and its salivary gland benefit needs to be confirmed in larger, more controlled studies. Early efforts have also been made to mitigate kidney damage of PSMA-targeted radiopharmaceuticals with radical scavenger and radioprotector α1-microglobulin [54, 55]. These experiments yielded mixed results but warrant further study.

The kidneys are thought to be a potentially dose-limiting organ for PSMA radioligands [11, 21–23] based on an estimated critical radiation dose of 28 Gy above which risk of chronic renal disease appears to increase over time [43]. As mentioned, severe nephrotoxicity has generally not been observed in the mCRPC patients treated with PSMA radioligand therapies to date. This may be due in part to insufficient follow-up given that survival times in these patients are on the order of only 1–2 years, whereas radiation-induced kidney failure manifests in about 2 or more years [56]. In the case of the only approved therapy, [177Lu]Lu-PSMA-617, it is perhaps more likely that the cumulative radiation absorbed dose to the kidneys is below the critical threshold. Per its label, the cumulative radiation absorbed dose to the kidneys after administration of 6×7.4GBq [177Lu]Lu-PSMA-617 was calculated to be 19 Gy [5].

Nevertheless, PSMA radioligand therapies deployed in earlier disease settings, or in tandem with alpha-emitting agents (2, 57–58), could create the need to lower the cumulative dose to the kidneys. Alpha-emitting radionuclides appear to be more effective than their beta counterparts, but also carry greater risk of severe xerostomia and nephrotoxicity even in late stage mCRPC patients [2, 58]. In addition, PSMA radioligand therapy delivers higher doses to healthy organs in patients with lower tumor volumes [59]. Thus, patients with low tumor burden or those exhibiting regression after their first treatment cycle(s) may be at greater risk for kidney and salivary gland toxicity in subsequent cycles.

The mechanism by which JHU-2545 preferentially distributes 2-PMPA to non-malignant tissues is unclear. Multiple factors may contribute to this empiric finding. Differences in passive diffusion vs. PSMA-mediated uptake in tumor vs. normal tissues could be important. It is possible that 2-PMPA uptake in tumor tissue is enriched via binding and internalization of cell-surface PSMA. JHU-2545 would not be subject to this process until converted to 2-PMPA. While circulating as parent prodrug, however, JHU-2545 distribution and tissue penetration may be driven more by passive diffusion given masking of charges by the prodrug moieties. This process likely explains improved delivery of 2-PMPA to kidneys and salivary glands via JHU-2545 administration vs. direct administration of equimolar 2-PMPA. However, drug delivery and diffusion of small molecules into solid tumors, particularly the core of solid tumors, may be hindered by extracellular matrix deposition and fibrosis, poor vascularization, and high interstitial fluid pressure [60, 61]. JHU-2545 may thus lose this pharmacokinetic advantage over 2-PMPA in tumor tissue while simultaneously being unable to benefit from active transport via PSMA binding/internalization even after extravasation. This balance shift in the relative importance of active vs. passive drug delivery mechanisms in normal vs. malignant tumors could help explain differential distribution of JHU-2545 relative to 2-PMPA. Another possible contributing factor is differential cellular efflux of JHU-2545 vs. 2-PMPA.

One important limitation of this work relates to clinical translation. Human biology could differ from these model systems such that preferential delivery of 2-PMPA afforded by JHU-2545 is changed. For example, pre-administration of monosodium glutamate in a mouse model of prostate cancer appeared to show preferential shielding of kidney and salivary glands vs. tumor [62], but this finding was not replicated in the clinic [63]. It is important to note that, in contrast to JHU-2545, there have been no reports of differential pharmacokinetic distribution of monosodium glutamate to support the preclinical findings. Regardless, optimization of a clinical JHU-2545 dose and regimen to ensure shielding of healthy tissues without hindering tumor uptake may not be straightforward. These efforts, which are now the subject of a Phase 1 imaging sub-study (NCT06217822), would be aided by preclinical studies examining JHU-2545 effects on safety and efficacy of PSMA radioligand therapies.

This effort would also benefit from replication of the current study in multiple cell lines and in other model systems such as patient-derived xenografts. Mouse pharmacokinetic and imaging experiments in this study employed C4-2 and 22RV1 xenografts. Both cell lines are established mCRPC models, have been shown through various methods to express PSMA, and have been found to take up PSMA radioligands [64–66]. However, use of additional models and possibly correlation of preferential 2-PMPA tissue distribution mediated by JHU-2545 with varying PSMA expression levels would be informative. Given the debate surrounding potential contribution of glutamate carboxypeptidase III (GCPIII) binding to PSMA radioligand uptake [67–68], a possible role for this protein in the effect of JHU-2545 also warrants further investigation.

Conclusion

If the present findings are replicated in clinical studies, JHU-2545 pre-treatment could enable broader, more effective use of PSMA radioligand therapies.

Acknowledgements This research was supported by a Maryland TEDCO MII award, a grant from the National Multiple Sclerosis Society, and a grant from NCI R01CA161056 (to BSS) as well as the Institute of Organic Chemistry and Biochemistry of the Czech Academy of

Sciences v.v.i. (RVO 61388963). and the National Institute for Cancer Research (Programme EXCELES, ID Project No. LX22NPO5102). DA and DLT were supported in part by NIH/NCI R01CA201035. This work was also supported in part by NIH NCI R01CA229893 and R01CA240711 (DLT). We thank the JHU PET Center for providing ^{18}F-DCFPyL.

Author contributions MTN, BSS, and CK conceived the concept, contributed to rodent experimental designs, and wrote the manuscript. PM and AJ designed and synthesized JHU-2545. MTN, RPD, YW, EYC, RSL, and RR conducted the rodent pharmacokinetic studies and bioanalysis. DA, MFP, AN, AAC, JB, and DLT conducted the rodent imaging studies.

Declarations

Ethical approval No research in the present article involved human participants. All animal experiments were conducted in compliance with National Institutes of Health (NIH) guidelines and with the approval of the Institutional Animal Care and Use Committees at relevant institutions as detailed above.

Conflicts of interest Authors BSS, PM, AJ and RR are listed as inventors in patent applications filed by Johns Hopkins Technology Ventures covering novel compositions of 2-PMPA-based prodrugs including JHU-2545. MTN, BSS, RR, and CK are inventors on a method of use patent application filed by Johns Hopkins Technology Ventures covering PSMA normal tissue shielding. MTN, BSS, and RR co-founded Adarga Pharmaceuticals to commercialize these inventions which were licensed to Bayer AG and have received and/or are eligible for related milestone or royalty payments. This arrangement has been reviewed and approved by the Johns Hopkins University in accordance with its conflict of interest policies. Other authors declare no conflicts of interest exist.

References

1. Fendler WP, Rahbar K, Herrmann K, Kratochwil C, Eiber M. (177)Lu-PSMA Radioligand therapy for prostate Cancer. J Nucl Med. 2017;58:1196–200.
2. Kratochwil C, Bruchertseifer F, Rathke H, et al. Targeted alpha-therapy of metastatic castration-resistant prostate Cancer with (225)Ac-PSMA-617: swimmer-plot analysis suggests Efficacy regarding duration of Tumor Control. J Nucl Med. 2018;59:795–802.
3. von Eyben FE, Roviello G, Kiljunen T et al. Third-line treatment and (177)Lu-PSMA radioligand therapy of metastatic castration-resistant prostate cancer: a systematic review. Eur J Nucl Med Mol Imaging. 2017.
4. Sartor O, de Bono J, Chi KN, et al. Lutetium-177–PSMA-617 for metastatic castration-resistant prostate Cancer. N Engl J Med. 2021;385:1091–103.
5. Pluvicto (lutetium Lu. 177 vipivotide tetraxetan) [package insert]. Basel, Switzerland: Novartis AG; 2022.
6. Bouchelouche K, Turkbey B, Choyke PL. PSMA PET and Radionuclide Therapy in prostate Cancer. Semin Nucl Med. 2016;46:522–35.
7. Ristau BT, O'Keefe DS, Bacich DJ. The prostate-specific membrane antigen: lessons and current clinical implications from 20 years of research. Urol Oncol. 2014;32:272–9.
8. Eiber M, Fendler WP, Rowe SP, Calais J, Hofman MS, Maurer T, et al. Prostate-Specific Membrane Antigen Ligands for Imaging and Therapy. J Nucl Med. 2017;58:s67–76.
9. Virgolini I, Decristoforo C, Haug A, Fanti S, Uprimny C. Current status of theranostics in prostate cancer. Eur J Nucl Med Mol Imaging. 2018;45:471–95.
10. Afshar-Oromieh A, Babich JW, Kratochwil C, et al. The rise of PSMA ligands for diagnosis and therapy of prostate Cancer. J Nucl Med. 2016;57:s79–89.
11. Kratochwil C, Giesel FL, Stefanova M, et al. PSMA-Targeted Radionuclide Therapy of Metastatic Castration-resistant prostate Cancer with 177Lu-Labeled PSMA-617. J Nucl Med. 2016;57:1170–6.
12. AlSadi R, Bouhali O, Dewji S, Djekidel M. 177Lu-PSMA therapy for metastatic castration-resistant prostate Cancer: a Mini-review of State-of-the-art. Oncologist. 2022;27:e957–66.
13. Rahbar K, Ahmadzadehfar H, Kratochwil C, et al. German Multicenter Study investigating 177Lu-PSMA-617 Radioligand therapy in advanced prostate Cancer patients. J Nucl Med. 2017;58:85–90.
14. Hofman MS, Violet J, Hicks RJ et al. [(177)Lu]-PSMA-617 radionuclide treatment in patients with metastatic castration-resistant prostate cancer (LuPSMA trial): a single-centre, single-arm, phase 2 study. Lancet Oncol. 2018.
15. O'Keefe DS, Bacich DJ, Heston WD. Comparative analysis of prostate-specific membrane antigen (PSMA) versus a prostate-specific membrane antigen-like gene. Prostate. 2004;58:200–10.
16. Silver DA, Pellicer I, Fair WR, Heston WD, Cordon-Cardo C. Prostate-specific membrane antigen expression in normal and malignant human tissues. Clin Cancer Res. 1997;3:81–5.
17. Taieb D, Foletti JM, Bardies M, Rocchi P, Hicks R, Haberkorn U. PSMA-Targeted Radionuclide Therapy and salivary gland toxicity: why does it matter? J Nucl Med. 2018.
18. Ling SW, de Blois E, Hooijman E, van der Veldt A, Brabander T. Advances in 177Lu-PSMA and 225Ac-PSMA Radionuclide Therapy for metastatic castration-resistant prostate Cancer. Pharmaceutics. 2022;14:2166.
19. Feurecker B, Tauber R, Knorr K, et al. Activity and adverse events of actinium-225-PSMA-617 in Advanced Metastatic Castration-resistant prostate Cancer after failure of Lutetium-177-PSMA. Eur Urol. 2021;79:343–50.
20. Kabasakal L, AbuQbeitah M, Aygun A, et al. Pre-therapeutic dosimetry of normal organs and tissues of (177)Lu-PSMA-617 prostate-specific membrane antigen (PSMA) inhibitor in patients with castration-resistant prostate cancer. Eur J Nucl Med Mol Imaging. 2015;42:1976–83.
21. Kratochwil C, Giesel FL, Leotta K, et al. PMPA for nephroprotection in PSMA-targeted radionuclide therapy of prostate cancer. J Nucl Med. 2015;56:293–8.
22. Zechmann CM, Afshar-Oromieh A, Armor T, et al. Radiation dosimetry and first therapy results with a (124)I/ (131)I-labeled small molecule (MIP-1095) targeting PSMA for prostate cancer therapy. Eur J Nucl Med Mol Imaging. 2014;41:1280–92.

23. Kratochwil C, Bruchertseifer F, Rathke H et al. Targeted alpha therapy of mCRPC with 225Actinium-PSMA-617: Dosimetry estimate and empirical dose finding. J Nucl Med. 2017.
24. Chatalic KL, Heskamp S, Konijnenberg M, et al. Towards Personalized treatment of prostate Cancer: PSMA I&T, a promising prostate-specific membrane Antigen-targeted Theranostic Agent. Theranostics. 2016;6:849–61.
25. Maurer T, Eiber M, Schwaiger M, Gschwend JE. Current use of PSMA-PET in prostate cancer management. Nat Rev Urol. 2016;13:226–35.
26. Yordanova A, Becker A, Eppard E, et al. The impact of repeated cycles of radioligand therapy using [177Lu]Lu-PSMA-617 on renal function in patients with hormone refractory metastatic prostate cancer. Eur J Nucl Med Mol Imaging. 2017;44:1473–9.
27. Delker A, Fendler WP, Kratochwil C, et al. Dosimetry for (177) Lu-DKFZ-PSMA-617: a new radiopharmaceutical for the treatment of metastatic prostate cancer. Eur J Nucl Med Mol Imaging. 2016;43:42–51.
28. Baum RP, Kulkarni HR, Schuchardt C, et al. 177Lu-Labeled prostate-specific membrane Antigen Radioligand Therapy of Metastatic Castration-resistant prostate Cancer: Safety and Efficacy. J Nucl Med. 2016;57:1006–13.
29. Roll W, Brauer A, Weckesser M, Bogemann M, Rahbar K. Long-term survival and excellent response to repeated 177Lu-Prostate-specific membrane Antigen 617 Radioligand Therapy in a patient with Advanced Metastatic Castration-resistant prostate Cancer. Clin Nucl Med. 2018.
30. Gallyamov M, Meyrick D, Barley J, Lenzo N. Renal outcomes of radioligand therapy: experience of 177lutetium-prostate-specific membrane antigen ligand therapy in metastatic castrate-resistant prostate cancer. Clin Kidney J. 2019;13:1049–55.
31. Kulkarni H, Schuchardt C, SINGH A, Langbein T, Baum R. Early initiation of Lu-177 PSMA radioligand therapy prolongs overall survival in metastatic prostate cancer. J Nucl Med. 2018;59:529.
32. Majer P, Jancarik A, Krecmerova M, et al. Discovery of orally available prodrugs of the glutamate carboxypeptidase II (GCPII) inhibitor 2-Phosphonomethylpentanedioic acid (2-PMPA). J Med Chem. 2016;59:2810–9.
33. Chen Y, Pullambhatla M, Foss CA, et al. 2-(3-{1-Carboxy-5-[(6-[18F]fluoro-pyridine-3-carbonyl)-amino]-pentyl}-ureido)-pentanedioic acid, [18F]DCFPyL, a PSMA-based PET imaging agent for prostate cancer. Clin Cancer Res. 2011;17:7645–53.
34. Rowe SP, Macura KJ, Mena E, et al. PSMA-Based [(18)F]DCFPyL PET/CT is Superior to Conventional Imaging for Lesion Detection in patients with metastatic prostate Cancer. Mol Imaging Biol. 2016;18:411–9.
35. Amor-Coarasa A, Kelly JM, Gruca M, et al. Continuation of comprehensive quality control of the itG 68Ge/68Ga generator and production of 68Ga-DOTATOC and 68Ga-PSMA-HBED-CC for clinical research studies. Nucl Med Biol. 2017;53:37–9.
36. Thorek DL, Watson PA, Lee SG, et al. Internalization of secreted antigen-targeted antibodies by the neonatal fc receptor for precision imaging of the androgen receptor axis. Sci Transl Med. 2016;8:367ra167.
37. Nedelcovych M, Dash RP, Tenora L, et al. Enhanced brain delivery of 2-(Phosphonomethyl)pentanedioic acid following Intranasal Administration of its gamma-substituted Ester Prodrugs. Mol Pharm. 2017;14:3248–57.
38. Fendler WP, Reinhardt S, Ilhan H, et al. Preliminary experience with dosimetry, response and patient reported outcome after 177Lu-PSMA-617 therapy for metastatic castration-resistant prostate cancer. Oncotarget. 2017;8:3581–90.
39. Hohberg M, Eschner W, Schmidt M, et al. Lacrimal glands may represent organs at Risk for Radionuclide Therapy of prostate Cancer with [(177)Lu]DKFZ-PSMA-617. Mol Imaging Biol. 2016;18:437–45.
40. Kabasakal L, Toklu T, Yeyin N, et al. Lu-177-PSMA-617 prostate-specific membrane Antigen inhibitor therapy in patients with castration-resistant prostate Cancer: Stability, Bio-distribution and Dosimetry. Mol Imaging Radionucl Ther. 2017;26:62–8.
41. Scarpa L, Buxbaum S, Kendler D, et al. The (68)Ga/(177)Lu theragnostic concept in PSMA targeting of castration-resistant prostate cancer: correlation of SUVmax values and absorbed dose estimates. Eur J Nucl Med Mol Imaging. 2017;44:788–800.
42. Yadav MP, Ballal S, Tripathi M, et al. Post-therapeutic dosimetry of 177Lu-DKFZ-PSMA-617 in the treatment of patients with metastatic castration-resistant prostate cancer. Nucl Med Commun. 2017;38:91–8.
43. Bodei L, Cremonesi M, Ferrari M, et al. Long-term evaluation of renal toxicity after peptide receptor radionuclide therapy with 90Y-DOTATOC and 177Lu-DOTATATE: the role of associated risk factors. Eur J Nucl Med Mol Imaging. 2008;35:1847–56.
44. Kopka K, Benesova M, Barinka C, Haberkorn U, Babich J. Glu-ureido-based inhibitors of prostate-specific membrane Antigen: lessons learned during the development of a Novel Class of Low-Molecular-Weight Theranostic Radiotracers. J Nucl Med. 2017;58:s17–26.
45. Kelly JM, Amor-Coarasa A, Nikolopoulou A, et al. Dual-target binding ligands with modulated pharmacokinetics for endoradiotherapy of prostate Cancer. J Nucl Med. 2017;58:1442–49.
46. Kelly JM, Amor-Coarasa A, Ponnala S, et al. Trifunctional PSMA-Targeting constructs for prostate Cancer with unprecedented localization to LNCaP tumors. Eur J Nucl Med Mol Imaging. 2018;45:1841–51.
47. Zang J, Fan X, Wang H et al. First-in-human study of (177)Lu-EB-PSMA-617 in patients with metastatic castration-resistant prostate cancer. Eur J Nucl Med Mol Imaging. 2018.
48. Schmidt A, Wirtz M, Farber SF, et al. Effect of Carbohydration on the Theranostic Tracer PSMA I&T. ACS Omega. 2018;3:8278–87.
49. Zang J, Liu Q, Sui H, et al. 177Lu-EB-PSMA Radioligand Therapy with escalating doses in patients with metastatic castration-resistant prostate Cancer. J Nucl Med. 2020;61:1772–8.
50. Kramer V, Fernandez R, Lehnert W, et al. Biodistribution and dosimetry of a single dose of albumin-binding ligand [177Lu] Lu-PSMA-ALB-56 in patients with mCRPC. Eur J Nucl Med Mol Imaging. 2021;48:893–903.
51. Matteucci F, Mezzenga E, Caroli P, et al. Reduction of (68)Ga-PSMA renal uptake with mannitol infusion: preliminary results. Eur J Nucl Med Mol Imaging. 2017;44:2189–94.
52. van Kalmthout LWM, Lam M, de Keizer B, et al. Impact of external cooling with icepacks on (68)Ga-PSMA uptake in salivary glands. EJNMMI Res. 2018;8:56.
53. Baum RP, Langbein T, Singh A, et al. Injection of Botulinum Toxin for preventing salivary gland toxicity after PSMA Radioligand Therapy: an empirical proof of a Promising Concept. Nucl Med Mol Imaging. 2018;52:80–1.
54. Kristiansson A, Timmermand OV, Altai M, et al. Hematological and renal toxicity in mice after three cycles of high activity [177Lu]Lu-PSMA-617 with or without human α1-microglobulin. Sci Rep. 2024;14(1):10787.
55. Kristiansson A, Orbom A, Ahlstedt J, et al. 177Lu-PSMA-617 therapy in mice, with or without the antioxidant α1-Microglobulin (A1M), including kidney damage Assessment using 99mTc-MAG3 imaging. Biomol. 2021;11(2):263.
56. Valkema R, Pauwels SA, Kvols LK, et al. Long-term follow-up of renal function after peptide receptor radiation therapy with (90) Y-DOTA(0),Tyr(3)-octreotide and (177)Lu-DOTA(0), Tyr(3)-octreotate. J Nucl Med. 2005;46:s83–91.
57. Haberkorn U, Giesel F, Morgenstern A, Kratochwil C. The future of Radioligand Therapy: alpha, beta, or both? J Nucl Med. 2017;58:1017–8.

58. Kratochwil C, Bruchertseifer F, Rathke H, et al. Targeted alpha-therapy of metastatic castration-resistant prostate Cancer with (225)Ac-PSMA-617: Dosimetry Estimate and Empiric Dose Finding. J Nucl Med. 2017;58:1624–31.
59. Gaertner FC, Halabi K, Ahmadzadehfar H, et al. Uptake of PSMA-ligands in normal tissues is dependent on tumor load in patients with prostate cancer. Oncotarget. 2017;8:55094–103.
60. Hauge A, Rofstad EK. Antifibrotic therapy to normalize the tumor microenvironment. J Transl Med. 2020;18:207.
61. Shemi A, Khvalevsky EZ, Gabai RM, et al. Multistep, effective drug distribution within solid tumors. Oncotarget. 2015;6:39564–77.
62. Rousseau E, Lau J, Kuo HT, et al. Monosodium glutamate reduces 68Ga-PSMA-11 uptake in salivary glands and kidneys in a preclinical prostate cancer model. J Nucl Med. 2018;59:1865–8.
63. Harsini S, Saprunoff H, Alden T, et al. The effects of monosodium glutamate on PSMA radiotracer uptake in men with recurrent prostate cancer: a prospective, randomized, double-blind, placebo-controlled intraindividual imaging study. J Nucl Med. 2021;62:81–7.
64. Gorges TM, Riethdorf S, Ahsen O, et al. Heterogeneous PSMA expression on circulating tumor cells - a potential basis for stratification and monitoring of PSMA-directed therapies in prostate cancer. Oncotarget. 2016;7(23):34930–41.
65. Piron S, Verhoeven J, De Coster E, et al. Impact of the molar activity and PSMA expression level on [18F]AlF-PSMA-11 uptake in prostate cancer. Sci Rep. 2021;11(1):22623.
66. Luckerath K, Wei L, Fendler WP, et al. Preclinical evaluation of PSMA expression in response to androgen receptor blockade for theranostics in prostate cancer. EJNMMI Res. 2018;8(1):96.
67. Lucaroni L, Georgiev T, Prodi E, et al. Cross-reactivity to glutamate carboxypeptidase III causes undesired salivary gland and kidney uptake of PSMA-targeted small-molecule radionuclide therapeutics. Eur J Nucl Med Mol Imaging. 2023;50(3):957–61.
68. Lee Z, Heston WD, Wang X, Basilion JP. GCP III is not the off-target for urea-based PSMA ligands. Eur J Nucl Med Mol Imaging. 2023;50(10):2944–96.

Authors and Affiliations

Michael T. Nedelcovych[1,2,13] · Ranjeet P. Dash[1,2] · Ying Wu[1] · Eun Yong Choi[3] · Rena S. Lapidus[3] · Pavel Majer[4] · Andrej Jančařík[4] · Diane Abou[5] · Marie-France Penet[6,7] · Anastasia Nikolopoulou[8] · Alex Amor-Coarasa[8] · John Babich[8] · Daniel L. Thorek[5] · Rana Rais[1,2] · Clemens Kratochwil[9] · Barbara S. Slusher[1,2,6,10,11,11,12,13]

✉ Michael T. Nedelcovych
mtnede@gmail.com

✉ Barbara S. Slusher
bslusher@jhmi.edu

[1] Johns Hopkins Drug Discovery, Johns Hopkins School of Medicine, Baltimore, MD 21205, USA

[2] Department of Neurology, Johns Hopkins School of Medicine, Baltimore, MD 21205, USA

[3] Translational Laboratory Shared Service, University of Maryland School of Medicine, 655 West Baltimore Street, Baltimore, MD 21201, USA

[4] Institute of Organic Chemistry and Biochemistry, Academy of Sciences of the Czech Republic v.v.i, Prague 166 10, Czech Republic

[5] Depatment of Radiology, Washington University School of Medicine, Saint Louis, MO 63110, USA

[6] Departments of Oncology, Johns Hopkins School of Medicine, Baltimore, MD 21205, USA

[7] Depatment of Radiology and Radiological Science, Johns Hopkins School of Medicine, Baltimore, MD 21205, USA

[8] Division of Radiopharmaceutical Sciences and MI(3), Department of Radiology, Weill Cornell Medicine, New York, NY, USA

[9] Department of Nuclear Medicine, University Hospital Heidelberg, Heidelberg, Germany

[10] Departments of Medicine, Johns Hopkins School of Medicine, Baltimore, MD 21205, USA

[11] Departments of Psychiatry, Johns Hopkins School of Medicine, Baltimore, MD 21205, USA

[12] Departments of Neuroscience, Johns Hopkins School of Medicine, Baltimore, MD 21205, USA

[13] Johns Hopkins Drug Discovery, 855 North Wolfe Street, Baltimore, Maryland 21205, USA